Acta Mechanica 149, 215–227 (2001)

ACTA MECHANICA

Thermal effects in externally pressurized porous conical bearings with variable viscosity

P. Sinha, P. Chandra, Kanpur, and **S. S. Bhartiya,** Mumbai, India

(Received September 23, 1994; revised September 20, 1999)

Summary. The present paper analyzes the porous constant gap externally pressurized conical bearings when the slider is rotating with uniform angular velocity. The lubricant is assumed to be incompressible, and its viscosity varies exponentially with temperature. The lubricant inertia due to rotation of the slider is considered but the convective inertia is neglected. The energy equation is used to determine the temperature generated in the lubricant film. The governing system of coupled momentum and energy equation is solved numerically, using finite difference method, to determine various bearing characteristics. It is observed that for the surfaces which are highly porous the inlet pressure decreases remarkably, resulting in reduced load capacity of the bearing, and the torque remains unaffected with respect to variation in the permeability.

Notation

c	specific heat of the fluid
D	dissipation parameter
E	a type of Eckert number
h	lubricant film thickness
h_p	thickness of the porous matrix
$H = h_p/h$	nondimensional thickness of the porous matrix
k	thermal conductivity
$\bar{k}$	permeability
L	load capacity of the bearing
M	torque on the bearing surface
p	gauge pressure
p^*	pressure in the porous matrix
Pr	Prandtl number
Q	flow rate
R	rotational parameter
Re	Reynolds number
Re*	modified Reynolds number
T	temperature of the lubricant
T_l, T_u	temperature of the pad and the slider, respectively
u, v, w	velocity components in the x, y and ϕ directions, respectively
u^*, v^*, w^*	velocity components in the porous matrix
U, V, W	reference quantities for the velocity components
x, y, ϕ	conical coordinate system
x_{in}, x_o	inlet, outlet positions
α	angle between stationary pad surface and a plane perpendicular to the bearing axis
β	viscosity-temperature exponent
η	viscosity of the lubricant

ϱ density of the lubricant
ν_o kinematic viscosity of the lubricant
η_o viscosity of the lubricant at pad temperature
ω angular velocity of the slider

A bar above a variable indicates a corresponding nondimensional quantity.

1 Introduction

Several researchers have attempted to study porous bearings with various geometries. Morgan and Cameron [1] were perhaps the first to study porous journal bearings. Their analytical work has been further investigated and extended by Cameron et al. [2]. The latter research indicated that for porous metal bearings full hydrodynamic conditions can be maintained up to a certain critical load, provided there is a sufficient supply of oil. Above this critical load, the eccentricity ratio approaches unity, implying that the shaft touches the inner surface of the bearing, and consequently hydrodynamic lubrication ceases. Howarth [3] has discussed both experimentally and theoretically the performance of an externally pressurized bearing using circular porous thrust pads. Shukla and Isa [4] discussed the characteristics of an externally pressurized porous thrust bearing with a power law lubricant. Roy and Biswal [5] investigated externally pressurized conical and squeeze film bearings with a viscoelastic lubricant and studied the effect of inertia and porosity of the bearing material.

No significant effort seems to have been made to analyze thoroughly the thermal effects in porous conical bearings. Thermal effects in externally pressurized non porous conical bearings have been analyzed in detail by Kennedy et al. [6]. The convection terms were dropped in the energy equation. In a subsequent paper Sinha and Rodkiewicz [7] considered convection as well as dissipation effects. In a further development Chandra et al. [8] studied the influence of convective inertia on the characteristics of a parallel gap conical bearing. In order to fully comprehend the effect of inertia, both the convection as well as the dissipation terms were retained in the energy equation. All these studies were made on non-porous conical bearings.

The present paper is thus devoted to the study of thermal effects in externally pressurized porous conical bearings with temperature dependent viscosity given by the relation

$$\eta = \eta_o \exp\left[-\beta(T - T_l)\right], \tag{1}$$

where η_o is the dynamic viscosity of the lubricant at pad temperature T_l. The gap between the slider and the pad is assumed to be constant. In view of the model suggested by Kennedy et al. [6] only rotational inertia is considered, and convective inertia terms are neglected. Similarly, in the energy equation it is assumed that the convective term is negligible as compared to the dissipation term (for details one may see the order of magnitude analyses and numerical examples in [6]). This work is thus a an extension of the work by Kennedy et al. [6].

2 Governing equations

The geometry of the problem is shown in Fig. 1. The problem considers the analysis of steady flow of an incompressible lubricant in the constant gap of a conical bearing externally pressurized through the central recess. The upper part of the bearing, the slider, rotates with constant angular velocity ω, and both parts of the bearing are maintained at constant but dif-

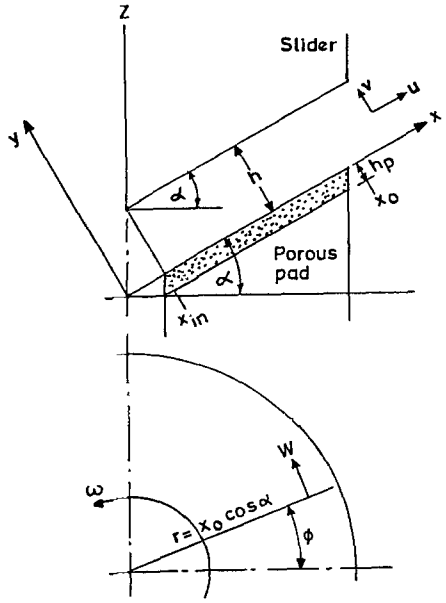

Fig. 1. Geometry of conical bearing with porous pad

ferent temperature, T_u and T_l for the upper and lower (pad) parts, respectively. The conical coordinate system x, y, ϕ is linked with the cylindrical coordinate system r, ϕ, z by the following transformation:

$$x = r\cos\alpha + z\sin\alpha\,, \qquad y = -r\sin\alpha + z\cos\alpha\,, \qquad \phi = \phi\,. \tag{2}$$

The gap between the slider and the pad is assumed to be constant. The pad is taken to be porous, and the bearing is fitted into the solid housing. It is assumed that the permeability of the porous pad is homogeneous and isotropic and the flow within it satisfies Darcy's law, i.e.

$$u^* = -\frac{k}{\eta}\frac{\partial p^*}{\partial x}\,, \tag{3}$$

$$v^* = -\frac{k}{\eta}\frac{\partial p^*}{\partial y}\,, \tag{4}$$

where k is the permeability, η is the viscosity of the lubricant, p^* is the pressure in the porous matrix, and u^* and v^* are velocities in the porous matrix in x- and y-direction, respectively. Further, $\partial p^*/\partial\phi = 0$ due to axial symmetry of the flow, thus $w^* = 0$.

Using the conical coordinate system (2) the continuity equation for flow in the porous pad is given by Kennedy et al. [6],

$$\frac{\partial u^*}{\partial x} + \frac{\partial v^*}{\partial y} + \frac{u^*\cos\alpha - v^*\sin\alpha}{x\cos\alpha - y\sin\alpha} = 0\,, \tag{5}$$

whereas the continuity equation for flow in the gap using relation (1) is given by Kennedy et al. [6],

$$\frac{\partial \bar{u}}{\partial \bar{x}} + \frac{\partial \bar{v}}{\partial \bar{y}} + \frac{\bar{u}}{\bar{x}} = 0\,. \tag{6}$$

It may be noticed that the continuity equation for the porous pad appears to be different from that for the gap. This happens because of the order of magnitude analysis for the gap (see the Appendix of [6]).

The other governing equations are

$$\text{Mom. } x \quad \frac{\partial^2 \bar{u}}{\partial \bar{y}^2} - \bar{\beta} \frac{\partial \bar{T}}{\partial \bar{y}} \frac{\partial \bar{u}}{\partial \bar{y}} = \exp\left[\bar{\beta}(\bar{T}-1)\right] \left[\frac{R\bar{w}^2}{\bar{x}} - \frac{d\bar{p}}{d\bar{x}}\right], \tag{7}$$

$$\text{Mom. } \phi \quad \frac{\partial^2 \bar{w}}{\partial \bar{y}^2} - \bar{\beta} \frac{\partial \bar{T}}{\partial \bar{y}} \frac{\partial \bar{w}}{\partial \bar{y}} = 0, \tag{8}$$

$$\text{Energy} \quad \frac{\partial^2 \bar{T}}{\partial \bar{y}^2} + D \exp\left[-\bar{\beta}(\bar{T}-1)\right] \left(\frac{\partial \bar{w}}{\partial \bar{y}}\right)^2 = 0, \tag{9}$$

where

$$\begin{aligned}
&\bar{x} = \frac{x}{x_o}, \quad \bar{y} = \frac{y}{h}, \quad \bar{u} = \frac{u}{U}, \quad \bar{v} = \frac{v}{V}, \quad \bar{w} = \frac{w}{W}, \quad U = \frac{Q}{2\pi x_o h \cos\alpha}, \\
&V = \frac{h}{x_o} U, \quad W = \omega x_o \cos\alpha, \quad \bar{T} = \frac{T}{T_l}, \quad \bar{\eta} = \frac{\eta}{\eta_o} = \exp\left[-\bar{\beta}(\bar{T}-1)\right], \\
&\bar{\beta} = \beta T_l, \quad \bar{p} = \frac{ph^2}{\eta_o x_o U}, \quad \nu_o = \frac{\eta_o}{\varrho}, \quad R = \frac{2\pi\omega^2 {x_o}^2 h^3 \cos^3\alpha}{\nu_o Q}, \\
&D = \frac{\mathrm{Pr}\, ER}{\mathrm{Re}^*}, \quad \mathrm{Re} = \frac{U x_o}{\nu_o}, \quad \mathrm{Re}^* = \mathrm{Re}\left(\frac{h}{x_o}\right)^2.
\end{aligned} \tag{10}$$

Further, using the nondimensional parameters,

$$\bar{k} = \frac{k}{{x_o}^2}, \qquad \bar{u}^* = \frac{u^*}{U}, \qquad \bar{v}^* = \frac{v^*}{V}, \qquad \bar{p}^* = \frac{p^* h^2}{\eta_o x_o U}, \tag{11}$$

Eqs. (3)–(5) transform to the following form:

$$\bar{u}^* = -\bar{k}\delta^2 \exp\left[\bar{\beta}(\bar{T}-1)\right] \frac{\partial \bar{p}^*}{\partial \bar{x}}, \tag{12}$$

$$\bar{v}^* = -\bar{k}\delta^4 \exp\left[\bar{\beta}(\bar{T}-1)\right] \frac{\partial \bar{p}^*}{\partial \bar{y}}, \tag{13}$$

$$\frac{\partial \bar{u}^*}{\partial \bar{x}} + \frac{\partial \bar{v}^*}{\partial \bar{y}} + \frac{\bar{u}^* \cos\alpha - \dfrac{\bar{v}^*}{\delta}\sin\alpha}{\bar{x}^* \cos\alpha - \dfrac{\bar{y}^*}{\delta}\sin\alpha} = 0, \tag{14}$$

where $\delta = x_o/h$.

Continuity requirements of flow in the porous matrix give the dimensionless equation

$$\frac{\partial^2 \bar{p}^*}{\partial \bar{x}^2} + \delta^2 \frac{\partial^2 \bar{p}^*}{\partial \bar{y}^2} + \frac{\left[\cos\alpha \dfrac{\partial \bar{p}^*}{\partial \bar{x}} - \delta \sin\alpha \dfrac{\partial \bar{p}^*}{\partial \bar{y}}\right]}{\bar{x}\cos\alpha} = 0, \tag{15}$$

where it is assumed that $\bar{x}\cos\alpha > (h/x_o)\,\bar{y}\sin\alpha$ as $h/x_o \ll 1$ and α is not close to 90°.

These equations are subject to the boundary conditions

$$\bar{u}(\bar{x}, 0) = \bar{u}(\bar{x}, 1) = 0. \tag{16}$$

Matching of the normal components of velocities at the interface ($\bar{y} = 0$) of the porous surface (pad) and the fluid film gives

$$\bar{v}(\bar{x}, 0) = \bar{v}^*(\bar{x}, 0). \tag{17}$$

Since the slider is taken to be non-porous, therefore

$$\bar{v}(\bar{x}, 1) = 0, \tag{18}$$

also

$$\begin{aligned} &\bar{w}(\bar{x}, 0) = 0, \qquad \bar{w}(\bar{x}, 1) = \bar{x}, \\ &\bar{T}(\bar{x}, 0) = 1, \qquad \bar{T}(\bar{x}, 1) = \bar{T}_u, \\ &\bar{u}^*(\bar{x}, -H) = \bar{v}^*(\bar{x}, -H) = 0, \\ &\bar{p}(1) = 0, \end{aligned} \tag{19}$$

where $H = h_p/h$, h_p is the thickness of the porous matrix.

The second condition in (19) implies fixed temperature boundary conditions. These conditions have been frequently used in recent years by several authors. A discussion in this regard is given by Saxena et al. [9].

The third condition in (19) implies that there is no flow across the porous matrix (i.e., at $y = -h_p$). This is justified since the porous matrix is assumed to be fitted in the solid housing.

Continuity of pressure at the interface ($\bar{y} = 0$) gives

$$\bar{p}(\bar{x}) = \bar{p}^*(\bar{x}, 0). \tag{20}$$

3 Method of solution

Since the peripheral length of the bearing is usually much larger than the thickness of the bearing shell, the pressure gradient in the porous matrix is assumed to be linear across the material of the bearing and is zero at the outer surface of the bearing, Mak and Conway [10]. This greatly simplifies the analysis. Thus, the following form of $\partial\bar{p}^*/\partial\bar{y}$ is assumed:

$$\frac{\partial \bar{p}^*}{\partial \bar{y}} = g(\bar{x})(\bar{y} + H). \tag{21}$$

It satisfies the condition that $\partial\bar{p}^*/\partial\bar{y} = 0$ at $\bar{y} = -H$, which shows that there is no flow of lubricant outside the porous matrix as the bearing is fitted into the housing.

Hence,

$$\bar{v}^*_{|\bar{y}=0} = -\bar{k}\delta^4 H g(\bar{x}). \tag{22}$$

Equation (15) along with Eq. (21) gives

$$g(\bar{x}) = -\frac{1}{\delta}\left[\frac{\partial^2 \bar{p}^*}{\partial \bar{x}^2} + \frac{1}{\bar{x}}\frac{\partial \bar{p}^*}{\partial \bar{x}}\right] \frac{\bar{x}\cos\alpha}{(\delta\bar{x}\cos\alpha - H\sin\alpha)}. \tag{23}$$

Thus, using the continuity of pressure at the interface of the oil and pad we get

$$\bar{v}^*_{|\bar{y}=0} = -\bar{k}\delta^3 H \frac{\cos\alpha}{(\delta\bar{x}\cos\alpha - H\sin\alpha)} \frac{d}{d\bar{x}}\left(\bar{x}\frac{d\bar{p}}{d\bar{x}}\right). \tag{24}$$

The continuity equation (6) with the help of boundary conditions (17) and (18) along with Eq. (24) gives the matching condition

$$\int_0^1 \bar{x}\bar{u}d\bar{y} = 1 - \bar{k}\delta^3 H\cos\alpha \int_{\bar{x}}^1 \left[\frac{\cos\alpha}{\delta s\cos\alpha - H\sin\alpha}\,\frac{d}{ds}\left(s\frac{d\bar{p}}{ds}\right)\right] ds\,, \tag{25}$$

where it is assumed that

$$\int_0^1 \bar{u}(\bar{x},\bar{y})\,d\bar{y} = 1 \quad \text{at} \quad \bar{x} = 1\,. \tag{26}$$

4 Numerical method

The system of Eqs. (7)–(9) has been discretized and solved simultaneously. Central difference representation has been used for the derivatives with respect to $\bar{y}$. Using the finite central difference scheme according to grid details shown in Fig. 2, Eqs. (8) and (9) can be written as follows:

$$\bar{w}(i,j) = \frac{1}{2}\left[\bar{w}(i,j+1) + \bar{w}(i,j-1)\right] - \frac{\bar{\beta}}{8}\left[\bar{w}(i,j+1) - \bar{w}(i,j-1)\right]\left[\bar{T}(i,j+1) - \bar{T}(i,j-1)\right], \tag{27}$$

$$\bar{T}(i,j) = \frac{1}{2}\left[\bar{T}(i,j+1) + \bar{T}(i,j-1)\right] + \frac{D}{8}\exp\left[-\bar{\beta}\left(\bar{T}(i,j) - 1\right)\right]\left[\bar{w}(i,j+1) - \bar{w}(i,j-1)\right]^2. \tag{28}$$

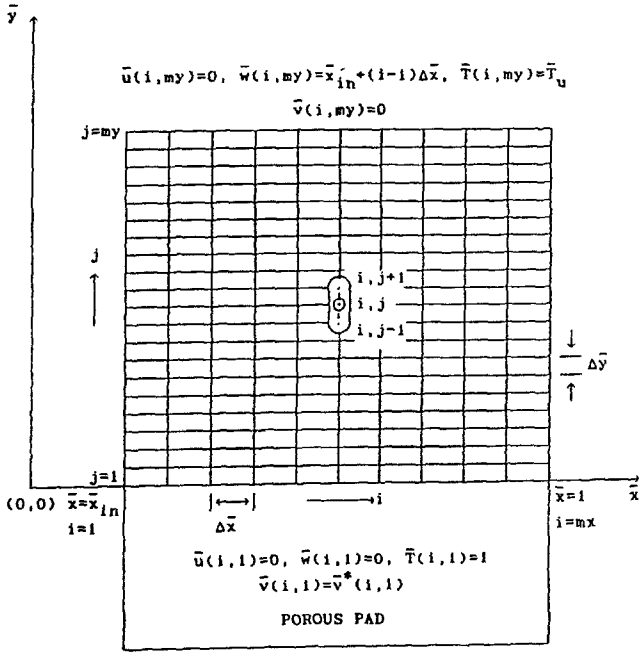

Fig. 2. Grid details

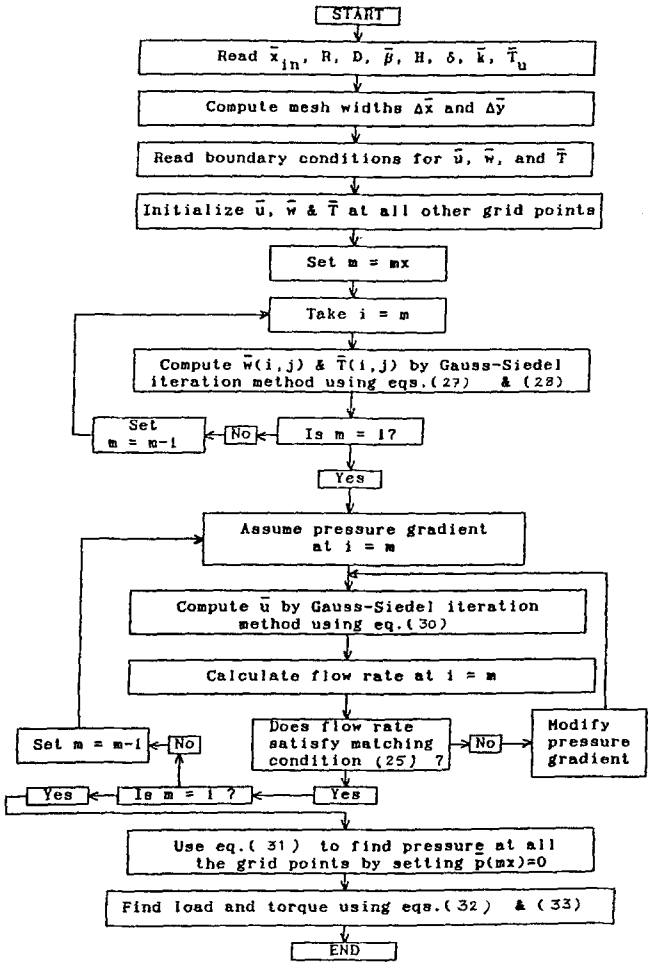

Fig. 3. Flow chart

A Gauss-Seidel iterative process is used to evaluate $\bar{w}(i,j)$ and $\bar{T}(i,j)$ as shown in the flow chart (Fig. 3) using the convergence criterion given by

$$\left|\frac{S_{\text{new}}(i,j) - S(i,j)}{S_{\text{new}}(i,j)}\right| \leq \varepsilon\,, \tag{29}$$

where S represents $\bar{u}, \bar{w}, \bar{T}$ and ε is the accuracy parameter.

Having found $\bar{w}(i,j)$ and $\bar{T}(i,j)$, Eq. (7) is solved for $\bar{u}(i,j)$ by assuming $d\bar{p}/(d\bar{x})\,(i)$ and using the finite central difference scheme

$$\begin{aligned}\bar{u}(i,j) = {} & \frac{1}{2}\left[\bar{u}(i,j+1) - \bar{u}(i,j-1)\right] \\ & - \frac{(\Delta\bar{y})^2}{2}\exp\left[\bar{\beta}\left(\bar{T}(i,j)-1\right)\right]\left[\frac{d\bar{p}}{d\bar{x}}(i) - R\,\frac{\left(\bar{w}(i,j)\right)^2}{\bar{x}(i)}\right] \\ & - \frac{\bar{\beta}}{8}\left[\bar{u}(i,j+1) - \bar{u}(i,j-1)\right]\left[\bar{T}(i,j+1) - \bar{T}(i,j-1)\right];\end{aligned} \tag{30}$$

$\bar{u}(i,j)$ are also determined using a Gauss-Seidel iteration process with the same convergence criterion. Marching begins from the outlet $(i = mx)$ to the inlet $(i = 1)$ assuming $d\bar{p}/(d\bar{x})\,(mx)$. The matching condition (25) is used to check the validity of the assumed pres-

sure gradient $d\bar{p}/(d\bar{x})\,(mx)$. If the assumed value of $d\bar{p}/(d\bar{x})\,(mx)$ fails to satisfy (25) at the outlet, its value is modified and the same procedure is repeated. Then we proceed to the grid point $i = mx - 1$ and the above mentioned procedure is repeated. This procedure is continued for each mesh point until (25) is satisfied for all points of the mesh, including the inlet ($i = 1$). A flow chart giving details of this method is shown in Fig. 3.

The above mentioned process determines not only the velocity distribution at each grid point but also the pressure gradient. Pressure is then found by using the forward difference formula

$$\bar{p}(i) = \bar{p}(i+1) - \Delta\bar{x}\,\frac{d\bar{p}}{d\bar{x}}\,(i)\,. \tag{31}$$

5 Load capacity and torque

Once the pressure distribution is known, the bearing characteristics, load capacity and torque of the bearing have been calculated by using the following formulae. The nondimensional load $\bar{L}$ of the bearing is given by

$$\bar{L} = \frac{lH^2}{\pi {x_0}^2 \eta_0 U \cos^2\alpha} = -\int_{\bar{x}_{in}}^{1} \left(\bar{x}^2 \frac{d\bar{p}}{d\bar{x}}\right) d\bar{x}\,, \tag{32}$$

and the nondimensional torque $\bar{M}$ of the bearing by

$$\bar{M} = \frac{Mh}{2\pi\eta_0 {x_0}^4 \omega \cos^3\alpha} = \int_{\bar{x}_{in}}^{1} \left[\bar{x}^2 \exp\left[-\bar{\beta}(\bar{T}-1)\right] \frac{\partial\bar{w}}{\partial\bar{y}}\right] d\bar{x}\,. \tag{33}$$

The integrals which appear in (32) and (33) are evaluated numerically by Simpson's rule using the previously obtained values of $d\bar{p}/d\bar{x}$ and $\bar{w}$.

6 Results and discussion

Numerical values for various bearing characteristics are obtained by taking $R = 60$, $\bar{x}_{in} = 0.10$ and $\bar{\beta} = 0, 1, 5$. H and δ are taken to be 10^2 and 2×10^3, respectively. The nondimensional permeability $\bar{k}$ varies from 0 to 1×10^{-10}. In the limiting case $\bar{k} = 0$, both the surfaces of the bearing become nonporous, and the present problem reduces to the one discussed by Kennedy et al. [6].

In accordance with Saxena et al. [9] the value of D has been taken as 1.5.

It has been observed by Kennedy et al. [6], and Chandra et al. [8] that cooling of the slider is advantageous, as it increases the load capacity and decreases the friction in the bearing. In view of this, results are presented for the case of cool slider-hot pad condition only, i.e. for $\bar{T}_u = 0.8$.

It is to be mentioned that in the present analysis values of $\bar{w}(\bar{x}, \bar{y})$ and $\bar{T}(\bar{x}, \bar{y})$ remain similar to those reported by Kennedy et al. [6]. This happens because Eqs. (27) and (28) do not involve the permeability parameter $\bar{k}$. So, these quantities have not been discussed here.

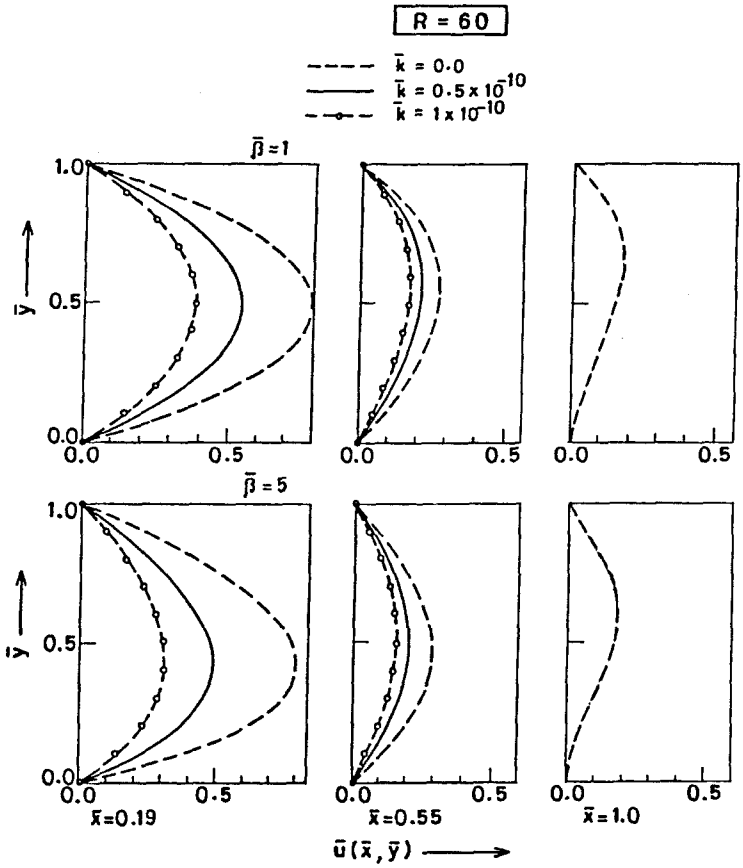

Fig. 4. Effect of permeability $\bar{k}$ on velocity distribution along $\bar{x}$ direction at different cross-sections for $R = 60$

6.1 Velocity distribution

Figures 4 ($R = 60$) and 5 ($R = 150$) show the effect of $\bar{k}$ on the velocity $\bar{u}(\bar{x}, \bar{y})$ at different cross-sections of the bearing for $\bar{\beta} = 1$ and 5. For $\bar{\beta} = 1$ as well as 5, the velocities $\bar{u}(\bar{x}, \bar{y})$ at all the values of $\bar{k}$ are highest near the inlet ($\bar{x} = 0.19$). For $\bar{\beta} = 1$, the velocity profile $\bar{u}(\bar{x}, \bar{y})$ appears to be symmetric about the centre line. Departure from the symmetric nature of the flow begins to appear from the central region (i.e., for $\bar{x} \geq 0.55$), and the lubricant in the upper half of the film is seen to move faster than that in the lower half. This behavior is most significant in the outlet region and is due to rotation of the slider. For $\bar{\beta} = 5$, the symmetric nature of the flow is slightly disturbed, and the lubricant near the pad seems to move faster. It is also observed that for a given $\bar{y}$ the value of $\bar{u}(\bar{x}, \bar{y})$ continuously decreases as the lubricant moves towards the outlet in case of $\bar{\beta} = 1$ as well as $\bar{\beta} = 5$. It happens due to the conical geometry of the problem which shows continuous increase in the area of cross-section through which the lubricant passes. These observations are similar to those of Kennedy et al. [6]. Further it is seen from Fig. 4 that $\bar{u}(\bar{x}, \bar{y})$ decreases as the permeability parameter $\bar{k}$ increases for all the values of $\bar{\beta}$ which may be due to the increased filtration with increase in $\bar{k}$. The decrease in $\bar{u}(\bar{x}, \bar{y})$ is more significant in the inlet zone. However, as the lubricant moves towards the outlet ($\bar{x} = 1.0$), the decrease in $\bar{u}(\bar{x}, \bar{y})$ becomes lesser, and at the outlet the curves for all values of $\bar{k}$ coincide. Numerical calculations yield negative velocities in the outlet

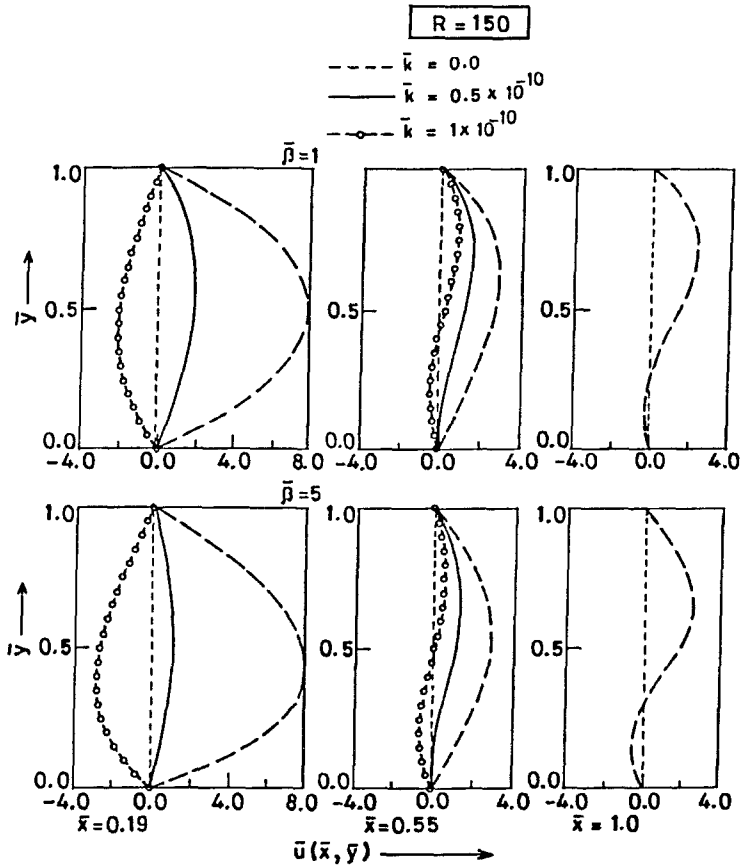

Fig. 5. Effect of permeability $\bar{k}$ on the velocity distribution along the $\bar{x}$-direction at different cross-sections for $R = 150$

region from $R = 80$ onwards. However, these values are so insignificant that the flow reversal cannot be depicted graphically.

As R is further increased to 150, the flow reversal becomes significant (Fig. 5) as was observed by Kennedy et al. [6]. For $R = 150, \bar{\beta} = 1$, there is no reversal of flow up to $\bar{k} = 0.5 \times 10^{-10}$. However, as $\bar{k}$ increases to 1×10^{-10}, there is a significant back-flow even in the mid region ($\bar{x} = 0.55$). This is because of the porous nature of the pad. At higher values of $\bar{k}$ a larger amount of lubricant is sucked in by the pad resulting in a decreased velocity of the lubricant in $\bar{x}$-direction in the fluid film region. At the outlet the lubricant at higher values of $\bar{k}$ moves forward to maintain the fixed flow rate according to relation (26), and the curves for all values of $\bar{k}$ become identical. Mathematically, this is justified in view of (25) and (26). It is also seen that at the outlet the depth to which the flow reversal penetrates from the stationary surfaces is reduced as compared to that in the mid region. At $R = 150, \bar{\beta} = 5$ similar flow behaviour is observed but the reversal of the flow is more prominent than that at $\bar{\beta} = 1$ and begins to appear from $\bar{k} = 0.5 \times 10^{-10}$ onwards.

6.2 Pressure distribution

Figures 6 ($\bar{\beta} = 0$), 7 ($\bar{\beta} = 1$) and 8 ($\beta = 5$) show the effect of $\bar{k}$ on the pressure distribution for $R = 60$. It is seen that commencing from the inlet the pressures continuously fall which is

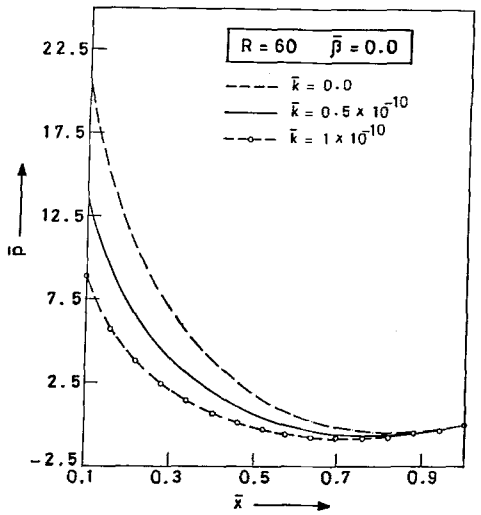

Fig. 6. Effect of permeability $\bar{k}$ on pressure distribution vs. $\bar{x}$ for $\bar{\beta} = 0$

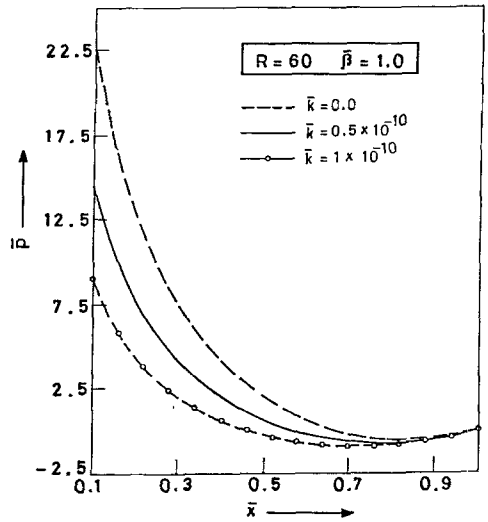

Fig. 7. Effect of permeability $\bar{k}$ on pressure distribution vs. $\bar{x}$ for $\bar{\beta} = 1$

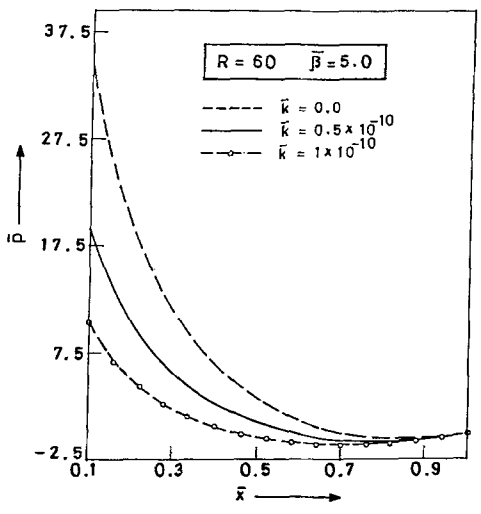

Fig. 8. Effect of permeability $\bar{k}$ on pressure distribution vs. $\bar{x}$ at $\bar{\beta} = 5$

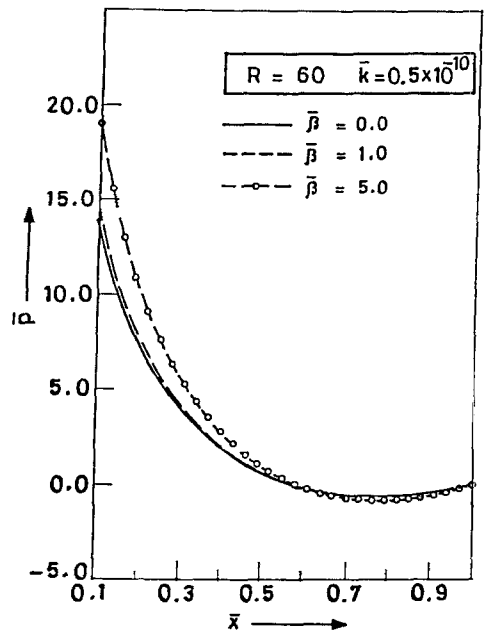

Fig. 9. Effect of $\bar{\beta}$ on pressure distribution at $R = 60$ and $\bar{k} = 0.5 \times 10^{-10}$

because of the viscous nature of the flow. The inlet pressure goes down significantly as $\bar{k}$ increases, both for $\bar{\beta} = 1$ and 5. This is understandable, since $\bar{u}(\bar{x}, \bar{y})$ decreases significantly with respect to $\bar{k}$ in the inlet region as was observed earlier (Fig. 4). Also, higher values of $\bar{k}$ indicate that a larger amount of lubricant enters in the porous pad through capillary action which results in a pressure drop in the fluid film region. Thus, it is likely that for the surfaces which are highly porous the pressure may reduce to such an extent that a film of the required thickness may not be maintained.

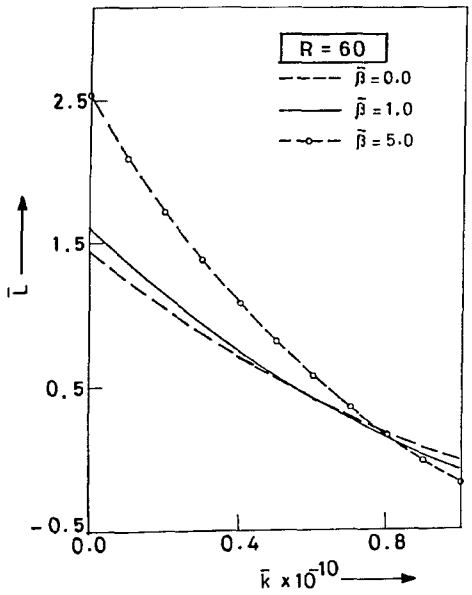

Fig. 10. Load capacity vs. permeability $\bar{k}$ for different values of $\bar{\beta}$

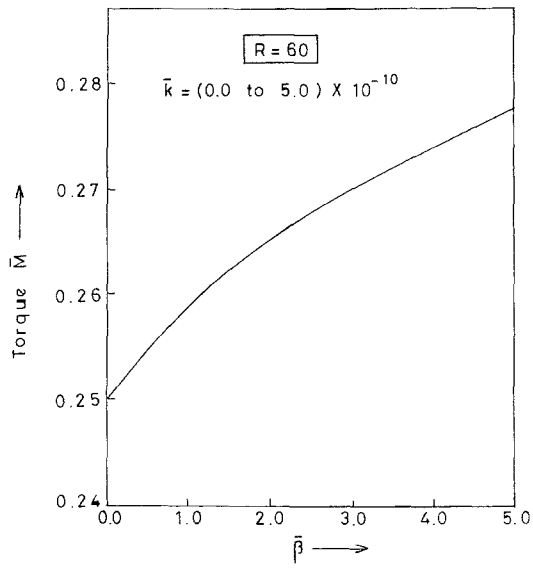

Fig. 11. Torque vs. viscosity coefficient $\bar{\beta}$ (independent of permeability $\bar{k}$)

The effect of $\bar{\beta}$ in the present case is similar to that observed by Kennedy et al. [6] in the nonporous case ($\bar{k} = 0$). Near the inlet, the pressures at $\bar{\beta} = 5$ are much higher than those at $\bar{\beta} = 1$ for all values of $\bar{k}$. This effect is not unexpected as a cool slider hot-pad situation is considered here, and cooling of the slider at higher values of $\bar{\beta}$ indicates the increase in viscosity of the lubricant close to the slider, which results in the higher pressure at higher values of $\bar{\beta}$.

Figure 9 shows that for $0.1 \leq \bar{x} \leq 0.6$ the pressure at $\bar{\beta} = 5$ is higher than that at $\bar{\beta} = 1$ for a fixed value of $\bar{k} = 0.5 \times 10^{-10}$. As $\bar{x}$ further increases, it becomes slightly lesser than those at $\bar{\beta} = 0$ and 1. However, this variation is not very significant.

6.3 Load capacity and torque

Figure 10 shows the load versus $\bar{k}$ for $R = 60$ and for different values of $\bar{\beta}$. It is seen that the load capacity of the bearing decreases with increase in $\bar{k}$. This is in view of the reduced pressure with an increase in $\bar{k}$ as observed earlier (Figs. 6–8). For $\bar{\beta} = 0$ the load capacity at $\bar{k} = 1 \times 10^{-10}$ is almost zero. It is also seen that at $\bar{\beta} = 5$ the load capacity is remarkably higher than that at $\bar{\beta} = 0$ and $\bar{\beta} = 1$ for $0 \leq \bar{k} \leq 0.8 \times 10^{-10}$. This happens due to higher pressures for $\bar{\beta} = 5$ as observed earlier. However, as $\bar{k}$ increases further, negative load capacities are observed, and the trend reverses, i.e. higher values of $\bar{\beta}$ show higher negative load capacity. It may happen due to lower pressures near the outlet at a particular value of $\bar{k} (= 0.5 \times 10^{-10})$ as seen in Fig. 9. Thus, it can be concluded that the porous nature of the pad may effect adversely, if the permeability is very high.

Figure 11 shows the torque of the bearing versus $\bar{\beta}$. It is seen from Eq. (33) that the torque is not effected by $\bar{k}$ as it depends upon $\bar{w}(\bar{x}, \bar{y})$ and $\bar{T}(\bar{x}, \bar{y})$, and it has already been said that both of these values remain unaffected by the permeability $\bar{k}$.

7 Conclusions

The present paper analyzes the porous constant gap externally pressurized conical bearings with temperature dependent viscosity. In the analysis, the lubricant inertia due to rotation of the slider is considered but convective inertia is neglected. The energy equation is used to determine the temperature generated in the lubricant film.

It can be concluded from the results and discussions that for the surfaces which are highly porous the inlet pressure decreases remarkably, resulting in reduced load capacity of the bearing. However, at lower values of the permeability parameter, the load capacity is found to be more for higher values of $\bar{\beta}$, but a reverse trend is observed at larger values of $\bar{k}$. Thus, the porous nature of the pad may not be favorable to the load capacity of an externally pressurized conical bearing. It is also seen that the torque of the bearing remains unaffected with respect to a variation in permeability.

References

[1] Morgan, V. T., Cameron, A.: Mechanism of lubrication in porous metal bearings. Proc. Inst. Mech. Engrs. **171,** 151–157 (1957).
[2] Cameron, A., Morgan, V. T., Stainsby, D.: Critical conditions for hydrodynamic lubrication of porous metal bearings. Proc. Inst. of Mech. Engrs. **176,** 761–770 (1962).
[3] Howarth, R. B.: Externally pressurized porous thrust bearings. ASLE Trans. **19,** 293–300 (1976).
[4] Shukla, J. B., Isa, M.: Externally pressurized porous thrust bearings with power law lubricants. Wear **33,** 85–92 (1975).
[5] Roy, J. S., Biswal, S.: Inertia effects in conical porous bearing with a viscoelastic lubricant. Wear **87,** 109–121 (1983).
[6] Kennedy, J. S., Sinha, P., Rodkiewicz, C. M.: Thermal effects in externally pressurized conical bearings with variable viscosity. Trans. ASME, J. Trib. **110,** 201–211 (1988).
[7] Sinha, P., Rodkiewicz, C. M.: Convection and dissipation effects in oil lubricated conical bearings with variable viscosity. Trans. ASME, J. Trib. **113,** 339–342 (1991).
[8] Chandra, P., Sinha, P., Saxena, S.: Effect of lubricant inertia in externally pressurized conical bearings with temperature dependent viscosity. Acta Mech. **106,** 157–171 (1994).
[9] Saxena, S., Chandra, P., Sinha, P.: THD analysis of non-constant gap, externally pressurized conical bearings. Tribology Trans. **38,** 438–444 (1995).
[10] Mak, W., Conway, H. D.: The lubrication of a long, porous, flexible journal bearing. Trans. ASME, J. Lub. Tech. **99,** 449–452 (1977).

Authors' addresses: P. Sinha, P. Chandra, Department of Mathematics, Indian Institute of Technology, Kanpur-208016 (E-mail: prawal@iitk.ernet.in); S. S. Bhartiya, Department of Mathematics, Indian Institute of Technology, Bombay, Powai, Mumbai-400076, India